The 2009 IEEE/RSJ International Conference on
Intelligent Robots and Systems
October 11-15, 2009 St. Louis, USA

Object Dynamics Virtualization by Robotic Assistance for Cooperative Object Handling with Human

Jun Ishikawa, Atsushi Sakai, and Katsuhisa Furuta, *Member, IEEE*

***Abstract*—This paper proposes an object dynamics virtualization that enables a human operator to handle the object easy for a given task by changing dynamics of the object by a robot assistance. The proposed method uses a force sensor fixed between an end effector of the manipulator and an object to measure force/torque applied by the manipulator to the object. Then, force/torque applied by an operator are estimated by using a disturbance observer, which subtracts the sensing force/torque from those calculated based on the object acceleration. Using the force sensor makes implementation easier by isolating the object dynamics from those of the manipulator. By using a virtual internal model driven by the estimated force/torque, a task-oriented mechanical impedance is given to the object that is in reality heavy and unbalanced as if it were lighter and well-balanced. Experiments to virtualize dynamics of a rod with a weight at one end, *i.e.*, an example of an unbalanced object, to be a uniform disc by a SCARA manipulator with three degrees-of-freedom were conducted, and the results showed the validity of the proposed method.**

I. Introduction

MECHANICAL impedance control [1] has played an important role in various robot applications, especially for cooperative motion control with human. It is common knowledge that the impedance control can be used to give compliance to manipulators making them flexible with external force/torque by humans. It is also used to make a mobile robot follow an operator with an appropriate impedance to carry an object cooperatively [2][3]. It is important for such impedance control to be designed to be task-oriented [4], and for example, a concept of task oriented virtual tools for teleoperation was proposed in [5]. In [6], apparent dynamics, *i.e.*, a task-oriented impedance for a handling object carried by a mobile robot and a human operator, was proposed.

It has been more than 20 years since disturbance observers (DOBs) were used in robotics [7], and now they are essentials to linearize manipulator nonlinear dynamics by feedback control. Regarding the impedance control, DOBs are used to eliminate modeling errors in order to realize precise compliant motion as designed [8][9]. Another way to use DOBs for the impedance control is to use them as a reaction force/torque observer [2] and for force-sensor-less impedance control [10]. It has been a challenge how precisely force/torque applied by humans or other external environments is measured, and its extension for power assist systems, for example, is a power-assisted wheel chair [11]. Reference [12] is an excellent paper to generally discuss those kinds of force-sensor-less power assist control.

The authors proposed a DOB using acceleration feedback for cancellation of pivot nonlinearities of hard disk drives [13], and the results implies that disturbance can be observed more easily and precisely by setting sensors closer to the source of the disturbance. This is also true of manipulators to hide their complicated dynamics and to more focus the disturbance estimation on a handling object itself. Thus, to realize a task-oriented object dynamics virtualization, in the proposed method, a force sensor is set between a manipulator and an object to estimate not disturbance, but external force/torque applied by an operator. An advantage of using a force sensor fitted at that location is that operators can handle the object at anywhere they like, unlike setting the sensor at a predetermined operator's handling point on the object. However, it should be noted that an easy implementation that uses sensing force/torque as those applied by the operator just after coordinate system transformation ignoring the object dynamics makes the whole control system less-damped or sometimes unstable especially when the object is handled with large acceleration. This issue is discussed in Section III.

The proposed method virtualizes real dynamics of an object to have another virtual mass, inertia tensor, mechanical impedance suitable for a given task based on a model following control using a virtual internal model (VIM) [14] driven by the estimated external force/torque. For example, a heavy and unbalanced object can be handled as if it were well-balanced and lighter than the real one. Model matching methods such a load sharing written in [15] could be alternatives, but the model following approach is adopted in this paper for the sake of good perspective of robustness in designing impedance with small or no damping. To show the validity of the proposed method, experiments are conducted using a selective compliance assembly robot arm (SCARA) type manipulator with three joints driven by direct drive motors. In the experiment, dynamics of a rod with a weight at one end, *i.e.*, an unbalanced object is virtualized to have a virtual dynamics as a uniform disc.

II. Object Dynamics Virtualization

A. Concept of the Virtualization

The objective here is to assist an operator who is handling

Manuscript received March 1, 2009.

J. Ishikawa is with the Department of Robotics and Mechatronics, School of Science and Technology for Future Life, Tokyo Denki University, 2-2, Kanda Nishiki-cho, Chiyoda-ku, Tokyo 101-8457, Japan (phone: +81-3-5280-3915; fax: +81-3-5280-3793; e-mail: ishikawa@fr.dendai.ac.jp).

A. Sakai is with SECOM Co, Ltd. from April 1, 2009.

K. Furuta is with Tokyo Denki University and is a Fellow of IEEE, a Distinguished Member of IEEE Control Systems Society.

an object with a robot or more specifically a manipulator so as to feel it lighter and easier to be handled than real one (Fig. 1). For example, to make the object felt lighter, a lighter virtual mass and/or virtual smaller gravity are introduced. Furthermore, an appropriate mechanical impedance to achieve the task should be given to the object [4][5]. Although it is important to discuss what kinds of dynamics should be design for an operator to easily and skillfully achieve a given task, it will be the future work in cooperation with the authors' group working on human adaptive mechatronics (HAM), which is a system that adapts itself to the operator's skill level to provide assistance to improve the humans' skill [16]. Therefore, as the first step to the goal, an object dynamics virtualization, which gives the object a virtual property with a virtual mass, inertia tensor, stiffness, and damping around a compliance center located at any position and orientation, is proposed in the following part.

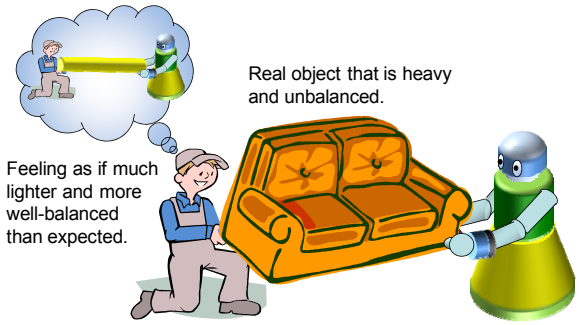

Fig. 1. Concept of object dynamics virtualization.

B. Impedance Control for Virtualization by Using Virtual Internal Model

Considering the case that a human operator and a manipulator cooperatively handle an object, four coordinate systems O, H, E, and B are defined as shown in Fig. 2. The coordinate system O is the Cartesian coordinate system, and those H, E, and B respectively show the handling point of the operator and that of the manipulator, and the center of gravity. Force/torque applied by the operator to the origin of H are defined as $F_a = \begin{bmatrix} \boldsymbol{f}_a{}^T & \boldsymbol{n}_a{}^T \end{bmatrix}^T \in \Re^6$ and force/torque by the manipulator at the origin of E as $F_m = \begin{bmatrix} \boldsymbol{f}_m{}^T & \boldsymbol{n}_m{}^T \end{bmatrix}^T \in \Re^6$. It is practical for a force sensor to be fixed at an end effector of the manipulator, not at the object itself. This is because objects can be quickly exchanged keeping the force sensor as it is. In such a case, however, object-handling force/torque should be carefully calculated in estimating ${}^H F_a$. Hereinafter, left superscripts indicate the coordinate system from which the variables are observed. Leaving the estimation problem until Section III, assume that the estimate is given as ${}^H \hat{F}_a$. Then, motion of a virtual object with a mechanical impedance in a virtual gravity $g_v \in \Re^3$, which is not necessary to be vertical, is generated by a virtual internal model. The virtual internal model generates a task-oriented dynamics different from those of the real object. Other coordinate systems G and

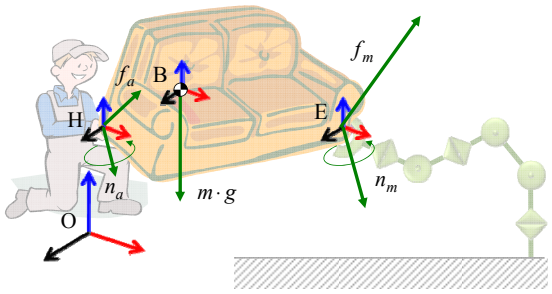

Fig. 2. Coordinate systems for a real object.

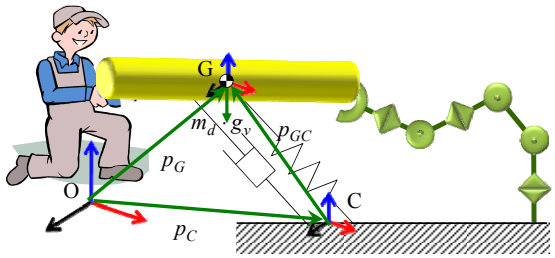

Fig. 3. Virtual object dynamics and the coordinate systems.

C, *i.e.*, respectively the center of the gravity of a virtual object and the compliance center, are defined as shown in Fig. 3.

Equivalent force/torque at the center of gravity G applied by the operator at the origin H is given by

$$ {}^G F_{Ga} = \begin{bmatrix} {}^G \boldsymbol{f}_{Ga} \\ {}^G \boldsymbol{n}_{Ga} \end{bmatrix} = \begin{bmatrix} {}^G R_H & O \\ \left[{}^G p_{HG} \times \right] {}^G R_H & {}^G R_H \end{bmatrix} {}^H \hat{F}_a , \tag{1} $$

where ${}^G R_H \in \Re^{3\times3}$ is a rotation matrix from the coordinate system H to G, ${}^G \boldsymbol{p}_{HG} \in \Re^3$ is a position vector of the origin H observed from the coordinate system G, and $\left[{}^G p_{HG} \times \right] \in \Re^{3\times3}$ is a skew symmetric matrix for cross product operation. The orientation of the object is determined by the Z-Y-Z Euler angle of the coordinate system. Thus, the position and orientation of the virtual object are defined as ${}^O \boldsymbol{p}_G = \begin{bmatrix} x_G & y_G & z_G \end{bmatrix}^T$ and ${}^O \boldsymbol{\varphi}_G = \begin{bmatrix} \phi_G & \theta_G & \psi_G \end{bmatrix}^T \in \Re^3$, respectively.

Then, the Newton's equation of motion based on the object coordinate system G of the virtual object, the mass and inertia tensor of which are m_d and ${}^G I_G$ with an impedance specified by the stiffness matrix $K_P = \mathrm{diag}\begin{pmatrix} k_{x_G} & k_{y_G} & k_{z_G} \end{pmatrix}$ and damping matrix $D_P = \mathrm{diag}\begin{pmatrix} d_{x_G} & d_{y_G} & d_{z_G} \end{pmatrix}$, is given by

$$ \begin{aligned} & m_d {}^G \ddot{\boldsymbol{p}}_G + D_P {}^G R_O {}^O \dot{\boldsymbol{p}}_{GC} + K_P {}^G R_O {}^O \boldsymbol{p}_{GC} \\ & = {}^G \boldsymbol{f}_{Ga} - m_d {}^G \boldsymbol{\omega}_G \times {}^G \dot{\boldsymbol{p}}_G + {}^G R_O \cdot {}^O \boldsymbol{g}_v \end{aligned} \tag{2} $$

where ${}^O \boldsymbol{p}_{GC} = {}^O \boldsymbol{p}_G - {}^O \boldsymbol{p}_C$.

To realize an orientation-selective impedance, an intermediate coordinate system S, which is derived by rotating the coordinate system C by $-\pi/2$ rad around the Y_C axis, is introduced (not depicted in Fig. 3). Then, an

orientation error of the coordinate system G to the coordinate system C is defined as

$$ {}^{S}\boldsymbol{\varphi}_{GC} = \begin{bmatrix} d\phi_G & d\theta_G - \dfrac{\pi}{2} & d\psi_G \end{bmatrix}^T \tag{3} $$

where ${}^{S}\boldsymbol{\varphi}_G = [d\phi_G \quad d\theta_G \quad d\psi_G]^T$ is the Z-Y-Z Euler angle of the coordinate system G from S. Then, define the angular velocity of the coordinate system G as ${}^{G}\boldsymbol{\omega}_G \in \Re^3$, the Euler's equation of motion is given by

$$ \begin{aligned} &{}^{G}I_G\,{}^{G}\dot{\boldsymbol{\omega}}_G + {}^{G}\boldsymbol{\omega}_G \times \left({}^{G}I_G\,{}^{G}\boldsymbol{\omega}_G\right) \\ &+ {}^{G}R_S \cdot {}^{S}R_{\Theta\Omega} \cdot D_\Theta \cdot {}^{S}R_{\Omega\Theta} \cdot \left({}^{S}R_G \cdot {}^{G}\boldsymbol{\omega}_G - {}^{S}R_O \cdot {}^{O}\boldsymbol{\omega}_C\right) \\ &+ {}^{G}R_S \cdot {}^{S}R_{\Theta\Omega} \cdot K_\Theta \cdot {}^{S}\boldsymbol{\varphi}_{GC} = {}^{G}\boldsymbol{n}_{Ga} \end{aligned} \tag{4} $$

where

$$ {}^{S}R_{\Theta\Omega} = \begin{bmatrix} 0 & -\sin d\phi_G & \cos d\phi_G \sin d\theta_G \\ 0 & \cos d\phi_G & \sin d\phi_G \sin d\theta_G \\ 1 & 0 & \cos d\theta_G \end{bmatrix}, \text{ and} \tag{5} $$

$$ {}^{S}R_{\Omega\Theta} = \frac{1}{\sin d\theta_G} \begin{bmatrix} -\cos d\phi_G \cos d\theta_G & -\sin d\phi_G \cos d\theta_G & \sin d\theta_G \\ -\sin d\phi_G \sin d\theta_G & \cos d\phi_G \sin d\theta_G & 0 \\ \cos d\phi_G & \sin d\phi_G & 0 \end{bmatrix}. \tag{6} $$

By introducing the orientation error ${}^{S}\boldsymbol{\varphi}_{GC}$, a selective compliance determined by $K_\Theta = \mathrm{diag}\left(k_{d\phi_G} \quad k_{d\theta_G} \quad k_{d\psi_G}\right)$ and $D_\Theta = \mathrm{diag}\left(d_{d\phi_G} \quad d_{d\theta_G} \quad d_{d\psi_G}\right)$ in three orthogonal directions around the coordinate systems C and S is realized.

When the directions of translational selective compliance are desirable to be based on the coordinate system C instead of G, (2) is replaced by

$$ \begin{aligned} &m_d\,{}^{G}\ddot{\boldsymbol{p}}_G + {}^{G}R_C D_P\,{}^{C}R_O\,{}^{O}\dot{\boldsymbol{p}}_{GC} + {}^{G}R_C K_P\,{}^{C}R_O\,{}^{O}\boldsymbol{p}_{GC} \\ &= {}^{G}\boldsymbol{f}_{Ga} - m_d\,{}^{G}\boldsymbol{\omega}_G \times {}^{G}\dot{\boldsymbol{p}}_G + {}^{G}R_O \cdot \boldsymbol{g}_v \end{aligned}. \tag{7} $$

Eventually, the motion of the virtual object to the externally-applied force/torque is given by

$$ \frac{d}{dt}\begin{bmatrix} {}^{O}\boldsymbol{p}_G \\ {}^{O}\boldsymbol{\varphi}_G \\ {}^{G}\dot{\boldsymbol{p}}_G \\ {}^{G}\boldsymbol{\omega}_G \end{bmatrix} = \begin{bmatrix} {}^{O}R_G\,{}^{G}\dot{\boldsymbol{p}}_G \\ {}^{O}R_{\Omega\Theta}\,{}^{O}R_G\,{}^{G}\boldsymbol{\omega}_G \\ m_d^{-1}F_G \\ {}^{G}I_G^{-1}N_G \end{bmatrix} \tag{8} $$

where ${}^{O}R_{\Omega\Theta}$ is the same one in (6) replacing $d\phi_G$ and $d\theta_G$ by ϕ_G and θ_G, and from (2) and (4),

$$ \begin{aligned} F_G = {}&{}^{G}\boldsymbol{f}_{Ga} - m_d\,{}^{G}\boldsymbol{\omega}_G \times {}^{G}\dot{\boldsymbol{p}}_G + {}^{G}R_O \cdot {}^{O}\boldsymbol{g}_v \\ &- D_P\,{}^{G}R_O\,{}^{O}\dot{\boldsymbol{p}}_{GC} - K_P\,{}^{G}R_O\,{}^{O}\boldsymbol{p}_{GC}, \text{ and} \end{aligned} \tag{9} $$

$$ \begin{aligned} N_G = {}&{}^{G}\boldsymbol{n}_{Ga} - {}^{G}\boldsymbol{\omega}_G \times \left({}^{G}I_G\,{}^{G}\boldsymbol{\omega}_G\right) \\ &- {}^{G}R_S \cdot {}^{S}R_{\Theta\Omega} \cdot D_\Theta \cdot {}^{S}R_{\Omega\Theta} \cdot \left({}^{S}R_G \cdot {}^{G}\boldsymbol{\omega}_G - {}^{S}R_O \cdot {}^{O}\boldsymbol{\omega}_C\right). \\ &- {}^{G}R_S \cdot {}^{S}R_{\Theta\Omega} \cdot K_\Theta \cdot {}^{S}\boldsymbol{\varphi}_{GC} \end{aligned} \tag{10} $$

To make the manipulator assist the operator and to virtualize the object dynamics, a model following control system is designed by using (8) as a virtual internal model. Due to the limitation of space, explanation of the controller design is omitted (see [17] for the detail).

III. Handling Force Estimation

A. Stability Analysis of Impedance Control

Consider a simple example of a mass system with one degree-of-freedom on a fiction-less base as shown in Fig. 4. For the system, an impedance control, the control input of which is f_m, is implemented for the external force f_a. As described above, a force sensor is desired to be attached between a manipulator and the object. Thus, assume that f_m can be measured. In such a case, an easy implementation where f_a is estimated as $\hat{f}_a = -Q(s) \cdot f_m$ ignoring the mass dynamics could be used, and an example of this kind of impedance control is described in Fig. 5. However, when the ratio of m_d to m is getting smaller and/or when the acceleration of the mass becomes large, it is necessary to use a disturbance observer to estimate f_a (Fig. 6).

Simple simulations with parameters in Table I were conducted to show that the easy implementation decreases stability margin as m_d is getting smaller from 15 to 1 kg when $m = 20$ kg. Here, the controller $C(s)$ consists of a first order lead-lag filter, and the 0dB crossover frequency are set to be $2\pi \cdot 15$ rad/s. Filter $Q(s)$ is a standard second order system, the parameters of which are also listed in Table I. Figures 7

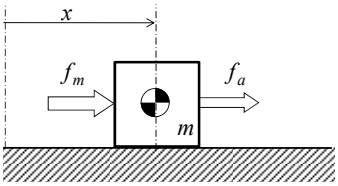

Fig. 4. Single mass system with one degree-of-freedom.

TABLE I
Simulation Parameters

Symbol	Numerical value	Remarks
m	20.0 kg	
m_d	15.0 kg	Heavy mass case for Fig. 7
d_d	66.0 N·s/m	Heavy mass case for Fig. 7
k_d	148 N/m	Heavy mass case for Fig. 7
m_d	1.00 kg	Light mass case for Fig. 8
d_d	4.40 N·s/m	Light mass case for Fig. 8
k_d	9.87 N/m	Light mass case for Fig. 8
ω_n	$2\pi \cdot 20$ rad/s	Natural frequency of $Q(s)$
ζ	1.20	Damping ratio of $Q(s)$

and 8 show frequency responses of a reference impedance model $V(s)$ and two transfer functions from f_a to x, *i.e.*,

$$V_{easy}(s)=\frac{P(s)C(s)\left[1+C(s)V(s)Q(s)\right]}{1+P(s)C(s)+C(s)V(s)Q(s)}, \qquad (11)$$

for the easy implementation, and

$$V_{DOB}(s)=\frac{P(s)\left[\left\{1-Q(s)\right\}+C(s)V(s)Q(s)\right]}{1+P(s)C(s)} \qquad (12)$$

for the DOB case. Here, $V(s)$ is designed for given m_d values so that the natural frequency and damping ratio are respectively to be π rad/s (0.5Hz) and 0.7. By comparing Figs. 7 and 8, it can be seen that the damping ratio of the transfer function from f_a to x in the easy implementation is decreasing as the ratio of m_d to m is getting smaller. Furthermore, the transfer function (11) became unstable when m_d = 1 kg while that of the DOB implementation (12) had almost all no influence of changing m_d on the stability. Thus, in implementing the object dynamics virtualization, DOB configurations should be used.

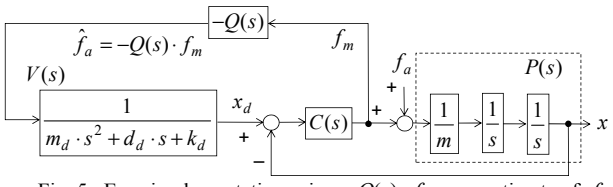

Fig. 5. Easy implementation using $-Q(s)\cdot f_m$ as an estimate of f_a.

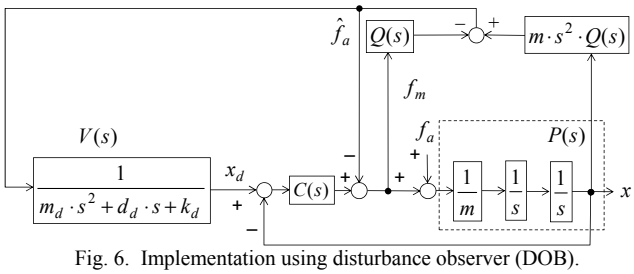

Fig. 6. Implementation using disturbance observer (DOB).

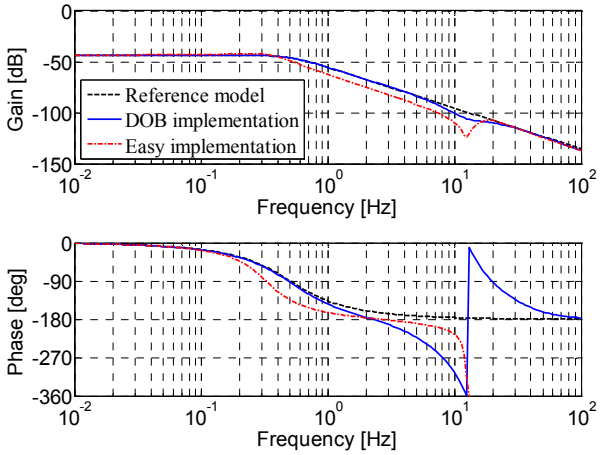

Fig. 7. Comparison of frequency responses of a reference model $V(s)$ and transfer functions from f_a to x when m = 20 kg: For m_d = 15 kg, there is no significant difference between two implementation methods.

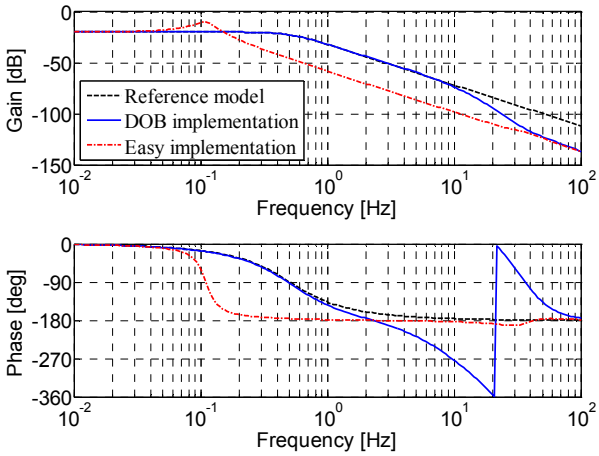

Fig. 8. Comparison of frequency responses of a reference model $V(s)$ and transfer functions from f_a to x when m = 20 kg: For m_d = 1 kg, the damping ratio in the easy implementation was 0.159, and it was much less than the designed value 0.7. Furthermore, $V_{easy}(s)$ was unstable.

B. Disturbance Observer (DOB) for Estimation of Handling Force/Torque Applied by Human Operator

This section concretely explains how to estimate force/torque applied by an operator based on a DOB. Here, definitions of coordinate systems are the same as those in Figs. 2 and 3. Force/torque applied by an manipulator are directly measured by a force sensor attached to the end effector, and the total equivalent force/torque applied to the center of gravity B are derived from the motion of the real object. Thus, the externally-applied force/torque by the operator can be calculated from the difference between those two kinds of force/torque.

Define the force/torque applied by the manipulator at the coordinate system E as ${}^{E}F_m=\left[{}^{E}\boldsymbol{f}_m{}^{T}\quad {}^{E}\boldsymbol{n}_m{}^{T}\right]^{T}$, equivalent forces/torques to the center of gravity B by the operator and by the manipulator are respectively given by

$${}^{B}F_{Ba}=\begin{bmatrix}{}^{B}\boldsymbol{f}_{Ba}\\ {}^{B}\boldsymbol{n}_{Ba}\end{bmatrix}=\begin{bmatrix}{}^{B}R_H & O\\ \left[{}^{B}p_{HB}\times\right]{}^{B}R_H & {}^{B}R_H\end{bmatrix}{}^{H}F_a, \text{ and} \qquad (13)$$

$${}^{B}F_{Bm}=\begin{bmatrix}{}^{B}\boldsymbol{f}_{Bm}\\ {}^{B}\boldsymbol{n}_{Bm}\end{bmatrix}=\begin{bmatrix}{}^{B}R_E & O\\ \left[{}^{B}p_{EB}\times\right]{}^{B}R_E & {}^{B}R_E\end{bmatrix}{}^{E}F_m. \qquad (14)$$

Newton and Euler's equation of motion of a real object, the mass and inertia tensor of which are defined as m and ${}^{B}I_B$, is given by

$$m\,{}^{B}\ddot{\boldsymbol{p}}_B={}^{B}\boldsymbol{f}_{Ba}+{}^{B}\boldsymbol{f}_{Bm}-m\cdot{}^{B}\boldsymbol{\omega}_B\times{}^{B}\dot{\boldsymbol{p}}_B+{}^{B}R_O\cdot{}^{O}\boldsymbol{g}, \text{ and} \qquad (15)$$

$${}^{B}I_B\,{}^{B}\dot{\boldsymbol{\omega}}_B+{}^{B}\boldsymbol{\omega}_B\times({}^{B}I_B\,{}^{B}\boldsymbol{\omega}_B)={}^{B}\boldsymbol{n}_{Ba}+{}^{B}\boldsymbol{n}_{Bm}. \qquad (16)$$

where ${}^{O}\boldsymbol{p}_B=\left[x_B\quad y_B\quad z_B\right]^{T}$ and ${}^{O}\boldsymbol{\varphi}_B=\left[\phi_B\quad \theta_B\quad \psi_B\right]^{T}$ are respectively the position and orientation of the real object, ${}^{B}\boldsymbol{\omega}_B\in\Re^3$ is the angular velocity observed from the

coordinate system B, and ${}^{O}\boldsymbol{g} \in \Re^3$ is the gravity vector observed from the Cartesian coordinate system O. Then, if the acceleration ${}^{B}\ddot{\boldsymbol{p}}_B$ and angular acceleration ${}^{B}\dot{\boldsymbol{\omega}}_B$ of the real object are measured, the equivalent force applied by the operator at B can be obtained as

$$ {}^{B}F_{Ba} = \begin{bmatrix} m\,{}^{B}\ddot{\boldsymbol{p}}_B - {}^{B}\boldsymbol{f}_{Bm} + m\,{}^{B}\boldsymbol{\omega}_B \times {}^{B}\dot{\boldsymbol{p}}_B - {}^{B}R_O \cdot {}^{O}\boldsymbol{g} \\ {}^{B}I_B\,{}^{B}\dot{\boldsymbol{\omega}}_B + {}^{B}\boldsymbol{\omega}_B \times ({}^{B}I_B\,{}^{B}\boldsymbol{\omega}_B) - {}^{B}\boldsymbol{n}_{Bm} \end{bmatrix}. \quad (17) $$

In the implementation, assume that the velocity ${}^{O}\dot{\boldsymbol{p}}_B$ and angular velocity ${}^{O}\dot{\boldsymbol{\varphi}}_B$ are available by a state observer or numerical finite difference based on the measurement of joint variables. Then, introducing filters $Q_i(s)$ ($i = 1,\ 2,\ \cdots,\ 12$) for a DOB as

$$ Q_i(s) = \frac{\omega_n^2}{s^2 + 2\zeta\omega_n s + \omega_n^2}, \quad (18) $$

the estimate of ${}^{B}F_{Ba}$ is given by

$$ {}^{B}\hat{F}_{Ba} = \begin{bmatrix} {}^{B}\hat{\boldsymbol{f}}_{Ba} \\ {}^{B}\hat{\boldsymbol{n}}_{Ba} \end{bmatrix} = \begin{bmatrix} m\,{}^{B}\ddot{\boldsymbol{p}}_B - {}^{B}\bar{\boldsymbol{f}}_{Bm} + m \cdot {}^{B}\boldsymbol{\omega}_B \times {}^{B}\dot{\boldsymbol{p}}_B - {}^{B}R_O \cdot {}^{O}\boldsymbol{g} \\ {}^{B}I_B\,{}^{B}\dot{\bar{\boldsymbol{\omega}}}_B + {}^{B}\boldsymbol{\omega}_B \times ({}^{B}I_B\,{}^{B}\boldsymbol{\omega}_B) - {}^{B}\bar{\boldsymbol{n}}_{Bm} \end{bmatrix} \quad (19) $$

where

$$ {}^{B}\ddot{\bar{\boldsymbol{p}}}_B = \mathrm{diag}\big(sQ_1(s) \quad sQ_2(s) \quad sQ_3(s)\big)\,{}^{B}R_O\,{}^{O}\dot{\boldsymbol{p}}_B, \quad (20) $$

$$ {}^{B}\boldsymbol{\omega}_B = {}^{B}R_O\,{}^{O}\tilde{R}_{\Theta\Omega}\,{}^{O}\dot{\boldsymbol{\varphi}}_B, \quad (21) $$

$$ {}^{B}\dot{\bar{\boldsymbol{\omega}}}_B = \mathrm{diag}\big(sQ_4(s) \quad sQ_5(s) \quad sQ_6(s)\big)\,{}^{B}\boldsymbol{\omega}_B, \quad (22) $$

$$ {}^{B}\bar{F}_{Bm} = \begin{bmatrix} {}^{B}\bar{\boldsymbol{f}}_{Bm} \\ {}^{B}\bar{\boldsymbol{n}}_{Bm} \end{bmatrix} = \mathrm{diag}\big(Q_7(s) \quad \cdots \quad Q_{12}(s)\big)\,{}^{B}F_{Bm}, \text{ and} \quad (23) $$

$$ {}^{O}\tilde{R}_{\Theta\Omega} = \begin{bmatrix} 0 & -\sin\phi_B & \cos\phi_B \sin\theta_B \\ 0 & \cos\phi_B & \sin\phi_B \sin\theta_B \\ 1 & 0 & \cos\theta_B \end{bmatrix}. \quad (24) $$

Eventually, the force/torque applied by the operator at the coordinate system H can be estimated as

$$ {}^{H}\hat{F}_a = \begin{bmatrix} {}^{H}R_B & O \\ [{}^{H}p_{BE}\times]\,{}^{H}R_B & {}^{H}R_B \end{bmatrix} {}^{B}\hat{F}_{Ba}. \quad (25) $$

Note that it is not essential that the location of the coordinate system H, *i.e.*, the handling point, should be uniquely identified. This is because ${}^{H}\hat{F}_a$ is only used to calculate ${}^{G}F_{Ga}$ in (1), and ${}^{G}F_{Ga}$ is directly calculate from ${}^{B}\hat{F}_{Ba}$ as

$$ {}^{G}F_{Ga} = \begin{bmatrix} {}^{G}\boldsymbol{f}_{Ga} \\ {}^{G}\boldsymbol{n}_{Ga} \end{bmatrix} = \begin{bmatrix} {}^{G}R_B & O \\ [{}^{G}p_{BG}\times]\,{}^{G}R_B & {}^{G}R_B \end{bmatrix} {}^{B}\hat{F}_{Ba} \quad (26) $$

This means that the number of handling points of the operator is not limited to one while all the other external force/torque are regarded to be valid for driving the impedance model.

IV. Experiment

A. Application for Manipulator with 3 Degrees-of-freedom

Figure 9 shows the coordinate systems of the SCARA manipulator with three degrees-of-freedom (DOF) used in the experiments. The position and orientation of the coordinate system E are respectively defined as ${}^{O}\boldsymbol{p}_E = [x_E \quad y_E \quad 0]^T$ and ${}^{O}\boldsymbol{\varphi}_E = [\phi_E \quad 0 \quad 0]^T$. In the experiments, the manipulator handles a rod with a weight at one end as an unbalanced real object as shown in Fig. 10. The virtual object, which is also shown in Fig. 10, is a disc with a diameter of 0.3 m. Figure 11 shows a close-up around the objects and the coordinate systems. The operator manipulates the object at the origin of the coordinate system H, and the objective here is to make the operator feel the real object as if a uniform disc. Kinematic parameters of the experimental system are listed in Table II.

TABLE II
KINEMATIC PARAMETERS OF EXPERIMENTAL SYSTEM

Symbol	Numerical value	Symbol	Numerical value
l_1	0.360 m	l_b	0.342 m
l_2	0.290 m	l_h	0.150 m
l_3	0.072 m	l_{g1}	0.115 m
		l_{g2}	0.023 m

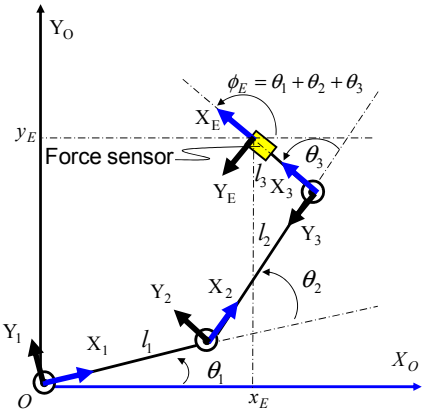

Fig. 9. Coordinate systems of a 3DOF manipulator.

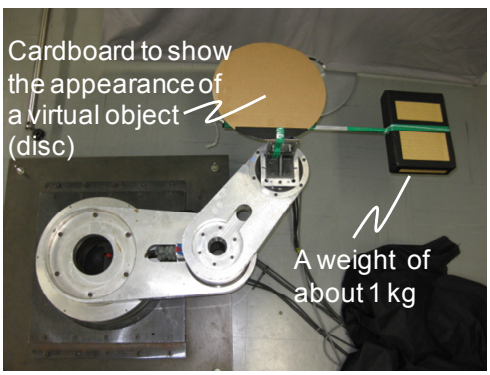

Fig. 10. Experimental system with 3 direct drive motors.

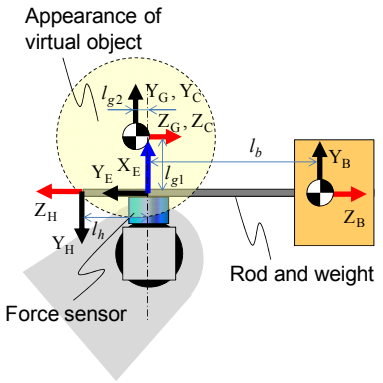

Fig. 11. Layout of real and virtual objects and the coordinate systems.

In the experimental system, the force/torque applied by the operator are estimated as

$$ {}^{B}\hat{F}_{Ba} = \begin{bmatrix} {}^{B}\hat{f}_{Bax} \\ {}^{B}\hat{f}_{Bay} \\ {}^{B}\hat{f}_{Baz} \\ {}^{B}\hat{n}_{Bax} \\ {}^{B}\hat{n}_{Bay} \\ {}^{B}\hat{n}_{Baz} \end{bmatrix} = \begin{bmatrix} 0 \\ m\,{}^{B}\ddot{y}_B - {}^{B}\bar{f}_{Bmy} - m\,{}^{B}\omega_{Bx}\cdot{}^{B}\dot{z}_B \\ m\,{}^{B}\ddot{z}_B - {}^{B}\bar{f}_{Bmz} + m\,{}^{B}\omega_{Bx}\cdot{}^{B}\dot{y}_B \\ {}^{B}I_{Bxx}\,{}^{B}\dot{\bar{\omega}}_{Bx} - {}^{B}\bar{n}_{Bmx} \\ 0 \\ 0 \end{bmatrix} \tag{27} $$

where

$$ \begin{bmatrix} {}^{B}\ddot{y}_B \\ {}^{B}\ddot{z}_B \end{bmatrix} = \begin{bmatrix} sQ_2(s) & 0 \\ 0 & sQ_3(s) \end{bmatrix} \begin{bmatrix} {}^{B}\dot{y}_B \\ {}^{B}\dot{z}_B \end{bmatrix} $$

$$ = \begin{bmatrix} sQ_2(s) & 0 \\ 0 & sQ_3(s) \end{bmatrix} \begin{bmatrix} \dot{x}_E\cos\phi_E + \dot{y}_E\sin\phi_E + l_b\dot{\phi}_E \\ \dot{x}_E\sin\phi_E - \dot{y}_E\cos\phi_E \end{bmatrix}, \text{ and} \tag{28} $$

$$ {}^{B}\dot{\bar{\omega}}_{Bx} = sQ_4(s)\left(-\dot{\phi}_E\right). \tag{29} $$

Here, ${}^{B}\bar{f}_{Bmy}$, ${}^{B}\bar{f}_{Bmz}$, and ${}^{B}\bar{n}_{Bmx}$ are derived by transforming the measured force/torque at E via (14) and then filtering. From ${}^{B}\hat{F}_{Ba}$ given by (27), ${}^{G}F_{Ga}$ is calculated by (26) and is used for generating the motion of the virtual object by the virtual internal model (8), where the calculations are conducted in the three dimensional space, and only horizontal components are used for reference trajectory generation. The manipulator used here is the same one in [17], and details of the model following control design, the sampling interval of which is 2 ms, are omitted.

Table III lists parameters of the real and virtual object, and two impedance models. One impedance model is for confirmation of the external force/torque estimation, and only the stiffness in Z_B direction is set to be much softer than the other directions, hereinafter referring as Experiment 1 (E1). The other impedance model is for virtualizing a uniform disc, the center of which is tightened at the compliance center C, referring as Experiment 2 (E2). In the experiment, the virtual mass m_d was set to be 15.0 kg, which was larger than that of the real object. This was because an object with such a weight

TABLE III
PARAMETERS OF OBJECTS AND DOB

Symbol	Numerical value	Remarks
m	1.12 kg	Mass of the rod and weight
${}^{B}I_{Bxx}$	1.57×10^{-2} kg·m^2	Moment of inertia of the rod and weight in the X_B direction
m_d	15.0 kg	Mass of the virtual object
${}^{G}I_{G}$	diag (16.9, 8.44, 8.44) $\times10^{-2}$ kg·m^2	Inertia tensor of the virtual object
D_P	diag (831, 831, 41.6) N·s /m	Translational damping in E1
K_P	diag (800, 800, 2.00) $\times10$ N/m	Translational stiffness in E1
D_Θ	diag (21.1, 21.1, 21.1) N·m·s /rad	Rotational damping in E1
K_Θ	diag (458, 458, 458) N·m /rad	Rotational stiffness in E1
D_P	diag (831, 831, 831) N·s /m	Translational damping in E2
K_P	diag (8.00, 8.00, 8.00) $\times10^3$ N/m	Translational stiffness in E2
D_Θ	diag (4.31, 4.31, 4.31) N·m·s /rad	Rotational damping in E2
K_Θ	diag (19.1, 19.1, 19.1) N·m /rad	Rotational stiffness in E2
ω_n	$2\pi\cdot10$ rad/s	Natural frequency of $Q_i(s)$
ζ	1.2	Damping ratio of $Q_i(s)$

of 15.0 kg was easy for the operator to handle the object, and it will be the future work to find what kinds of dynamics should be appropriate for given tasks.

B. Experimental Results

Figure 12 shows time responses of $-{}^{B}\bar{f}_{Bm}$, ${}^{B}\hat{f}_{Ba}$ and $m\,{}^{B}\ddot{z}_B$ in the translational compliant motion along Z_B axis in Experiment 1 (E1). From the figure, it was shown that $m\,{}^{B}\ddot{z}_B$ as dynamics of the real object should not be ignored and $-{}^{B}\bar{f}_{Bm}$ should not be used as a substitute for ${}^{B}\hat{f}_{Ba}$. In the lower half of Fig. 12, only $m\,{}^{B}\ddot{z}_B$ was plotted because the term of $m\,{}^{B}\omega_{Bx}\cdot{}^{B}\dot{y}_B$ in (27) was negligible small in E1. Another experiment based on an easy implementation where $-{}^{B}\bar{f}_{Bm}$ was used instead of ${}^{B}\hat{f}_{Ba}$ was conducted, and it was confirmed that the system became unstable in the easy implementation in the conditions of E1 in Table I.

Figure 13 shows time responses of ${}^{H}\hat{f}_{ay}$, ${}^{H}\hat{f}_{az}$, and ${}^{H}\hat{n}_{ax}$ in the rotational compliant motion in E2 when the operator intended to rotate the virtual object around the compliance center. Figure 14 shows the resultant trajectories of the origin of the coordinate system E in the X_O-Y_O plane and time responses of the orientation ϕ_E. Even if the real object was unbalanced, the reference trajectory was generated so that the operator could feel as if handling a disc fixed at a spindle although tracking performance of the control system was not so good. The reason why the tracking performance was poor was that disturbance cancelation and handling force compensation were omitted. This is because sensing and signal processing delays of the force sensor made the system unstable in the experimental system.

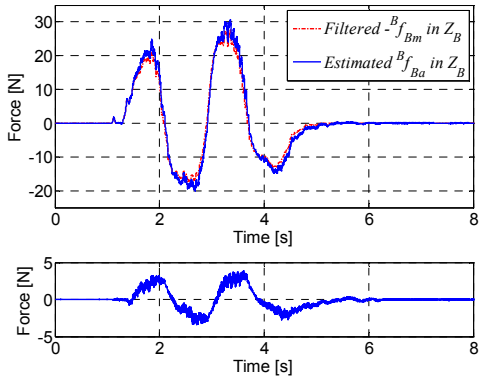

Fig. 12. Time responses of $-{}^{B}\bar{f}_{Bm}$, ${}^{B}\hat{f}_{Ba}$ and $m{}^{B}\ddot{\bar{z}}_{B}$ in the translational compliant motion along Z_B axis (E1).

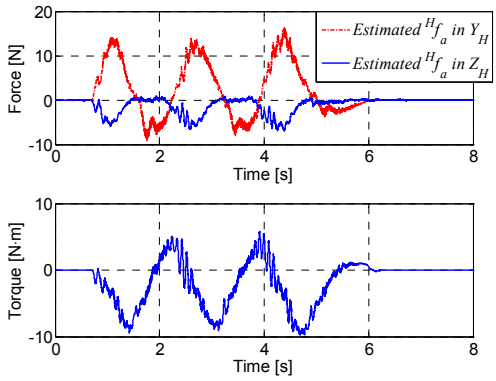

Fig. 13. Time responses of ${}^{H}\hat{f}_{ay}$, ${}^{H}\hat{f}_{az}$ and ${}^{H}\hat{n}_{ax}$ in the rotational compliant motion (E2).

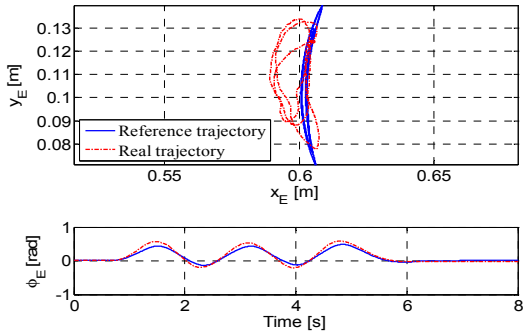

Fig. 14. Trajectories of the origin of the coordinate system E in the X_O-Y_O plane and time responses of the orientation ϕ_E in the rotational compliant motion (E2).

V. Conclusion

This paper proposed a virtualization of handling object dynamics to assist an operator who is handling the object with a manipulator. The propose method is based on DOB to estimate the external force/torque applied by the operator. Experiments were carried out using a SCARA type manipulator with three joints equipped with direct drive motors. The proposed method successfully virtualized dynamics of a rod with a weight at one end to have virtual dynamics as a uniform disc.

The future work will be to research what kinds of dynamics should be designed for an operator to easily and skillfully achieve given tasks. This will be conducted under the framework of the human adaptive mechatronics (HAM) that provides assisting mechanisms to improve the humans' skill.

References

[1] N. Hogan, "Impedance Control; An Approach to Manipulation, Part I, II, III," *the ASME Journal of Dynamic Systems, Measurement and Control*, vol.101, pp.1-24, 1985.

[2] S. Kobayashi, A. Muis, and K. Ohnishi, "Sensorless cooperation between human and mobile manipulator," *Proceedings of the IEEE International Conference on Industrial Technology*, pp. 811 – 816, 2005.

[3] Z. Wang, K. Fukaya, Y. Hirata, and K. Kosuge, "Impedance-based Motion Control of Passive-type Robot Porter for Handling an Object," *Proceedings of the IEEE International Conference on Robotics and Biomimetics* (*ROBIO '06*), pp. 709 – 714, 2006.

[4] K. Kosuge, and J. Ishikawa, "Task-Oriented Control of Single-Master Multi-Slave Manipulator System," *Robotics and Autonomous Systems*, vol. 12, pp. 95 – 105, 1994.

[5] T. Itoh, K. Kosuge, and T. Fukuda, "Human-machine cooperative telemanipulation with motion and force scaling using task-oriented virtual tool dynamics," *IEEE Transactions on Robotics and Automation*, vol. 16, no. 5, pp. 505 – 516 (2000).

[6] R. Suda, K. Kosuge, and H. Kakuya, "Object-impedance-based cooperative handling of object by mobile robot helper and human using visual and force information," *Proceedings. of the 2003 IEEE/ASME International Conference on Advanced Intelligent Mechatronics* (*AIM 2003*), vol. 1, pp. 592 – 597, 2003.

[7] M. Nakao, K. Ohnishi and K. Miyachi "A robust decentralize joint control based on interference estimation," *Proceedings of the IEEE International Conference on Robotics and Automation*, pp. 326 – 331, 1987.

[8] E. Leksono, T. Murakami, and K. Ohnishi, "Cooperative motion control of multimanipulator based on workspace disturbance observer with variable compliance gain," *Proceedings of the 23rd International Conference on Industrial Electronics, Control and Instrumentation* (*IECON 97*), vol. 3, pp. 1379 – 1384, 1997.

[9] R. Bickel, M. Tomizuka, and W. Chung, "Hybrid impedance control in constraint coordinates using a disturbance observer," *Proceedings of the 35th IEEE Conference on Decision and Control*, vo. 2, pp. 1974 – 1979, 1996.

[10] T. Murakami, R. Nakamura, F. Yu, and K. Ohnishi, "Force sensorless impedance control by disturbance observer," *Conference Record of the Power Conversion Conference*, pp. 352 – 357, 1993.

[11] S. Oh, N. Hata, and Y. Hori, "Integrated Motion Control of a Wheelchair in the Longitudinal, Lateral, and Pitch Directions," *IEEE Transactions on Industrial Electronics*, vol. 55, no. 4, pp. 1855 – 1862, 2008.

[12] S. Oh, and Y. Hori, "Generalized discussion on design of force-sensor-less Power Assist Control," *Proceedings of the 10th IEEE International Workshop on Advanced Motion Control 2008* (AMC '08), pp. 492 – 497, 2008.

[13] J. Ishikawa, and M. Tomizuka, "Pivot Friction Compensation Using an Accelerometer and a Disturbance Observer for Hard Disk Drives," *IEEE/ASME Transactions on Mechatronics*, vol. 3, no. 3, pp. 194 – 201, 1998.

[14] K. Kosuge, K. Furuta, and T. Yokoyama, "Virtual Internal Model Following Control of Robot Arms," *Proceedings of the 1987 IEEE International Conference on Robotics and Automation*, vol. 4, pp. 1549 – 1554, 1987.

[15] O. M. Al-Jarrah, and Y. F. Zheng, "Armmanipulator coordination for load sharing using variable compliance control," *Proceedings of the 1997 IEEE International Conference on Robotics and Automation*, pp. 895 – 900, 1997.

[16] K. Furuta, "Control of Pendulum: From Super Mechano-System to Human Adaptive Mechatronics," *Proceedings of the 42nd IEEE Conference on Decision and Control*, Plenary Talk., pp.1498-1507, 2003.

[17] J. Ishikawa, K. Kosuge, and K. Furuta, "Intelligent Control of Assembling Robot Using Vision Sensor," *Proceedings of the 1990 IEEE International Conference on Robotics and Automation*, vol. 3, pp. 1904 – 1909, 1990.